

1 **Title: Point-scale organic-matter decomposition in streambeds is weakly associated with reach-scale**
2 **respiration**

3

4 James C. Stegen^{1,2*}, Morgan Barnes¹, Dillman Delgado¹, Brieanne Forbes¹, Vanessa A. Garayburu-
5 Caruso¹, Amy E. Goldman¹, Maggi Laan^{1,3}, Sophia McKeever¹, Peter Regier¹, Lupita Renteria¹, Scott D.
6 Tiegs⁴

7 *Correspondence: James.Stegen@pnnl.gov

8 1. Pacific Northwest National Laboratory, Richland, WA, United States

9 2. Washington State University, Pullman, WA, United States

10 3. University of California, Riverside, CA, United States

11 4. Oakland University, Rochester, MI, United States

12

13 **Abstract**

14 Stream and river ecosystems play a central role in the movement and decomposition of particulate
15 organic matter, serving as a conduit between terrestrial hillslopes and coastal environments. Microbe-
16 catalyzed decomposition generates simpler organic molecules that fuel respiration, often in the
17 sediments of these ecosystems. However, the degree of connection between sediment-associated
18 respiration (ER_{sed}) and organic-matter-decomposition potential remains poorly understood. It is also
19 unclear whether organic-matter-decomposition potential is more closely associated with ER_{sed} , whole-
20 ecosystem respiration (ER_{tot}), or water-column respiration (ER_{wc}). We examined the link between
21 particulate organic-matter-decomposition potential—using cellulose-based cotton strips as a
22 standardized substrate—and all three components of respiration across 48 sites in the environmentally
23 diverse Yakima River Basin (Washington State, USA). We hypothesized that decomposition within
24 sediments would be most strongly related to ER_{sed} , but decomposition rates were more closely
25 associated with ER_{tot} , less so with ER_{sed} and not at all with ER_{wc} . This suggests that point-scale particulate
26 organic-matter-decomposition potential within stream/river sediments is more closely associated with
27 integrated system respiration rather than with processes confined to sediments or the water column
28 alone though these relationships were weak overall. Further, across the basin, decomposition rates
29 nearly spanned the previously reported global range for streams and rivers and were best explained by
30 total dissolved nitrogen (TDN), sediment grain size, and aridity of the upstream drainage area. These
31 results highlight the strong influence of land cover and basin-scale biophysical variation on sediment-
32 associated decomposition processes and indicate that mechanistic models of organic-matter
33 decomposition in streams and rivers should account for coupled sediment–water–land interactions.

34 **Key words:** Yakima River; organic-matter decomposition; sediment respiration; stream metabolism;
35 cotton-strip assay; hyporheic zone respiration

36

37

38 Introduction

39 Stream networks are major components of the global carbon cycle (Cole et al., 2007; Drake et al., 2018;
40 Talluto et al., 2024). Whole-stream metabolism is often studied as an integrated outcome of processes
41 occurring across the continuum from the air-water interface down through sediments that are below
42 the stream itself (Battin et al., 2023; Tank et al., 2010). The sediments include the interface between the
43 streambed and water column (i.e., the benthic zone) and the spatial domain below this interface,
44 referred to as the hyporheic zone (Boulton et al., 1998; Krause et al., 2011; Wondzell, 2011). The benthic
45 zone can be highly productive with significant primary producer (e.g., algae) and heterotrophic microbial
46 biomass (Allan et al., 2021). The hyporheic zone is also highly biogeochemically active due, in part, to
47 surface water flowing through it and mixing with groundwater to stimulate heterotrophic microbial
48 activity (Boano et al., 2014; Lewandowski et al., 2019; Zarnetske et al., 2011). Processes occurring on
49 and around sediments across the benthic-to-hyporheic continuum are often jointly responsible for the
50 bulk of biogeochemical activity in stream systems (Burrows et al., 2017; Fellows et al., 2001; Garayburu-
51 Caruso et al., 2025; Naegeli and Uehlinger, 1997), with important exceptions in large rivers (Roley et al.,
52 2023).

53 Metabolic processes within integrated stream systems are linked to the building of and breaking down
54 of organic matter (Hall and Hotchkiss, 2017a; Odum, 1956). Streams are commonly net heterotrophic,
55 meaning they mineralize more organic-matter-associated carbon than they fix by in-stream primary
56 production (Battin et al., 2023; Bernhardt et al., 2022). This emphasizes the importance of
57 understanding organic-matter decomposition in streams and its connection to respiration rates, which
58 are ultimately linked to rates of elemental cycling. Organic-matter decomposition is commonly
59 measured in stream systems by quantifying the breakdown of specific substrates (Benfield et al., 2017;
60 Woodward et al., 2012). Cellulose-based cotton strips are an increasingly common model substrate for
61 such studies as they enable broad comparisons across streams (and other types of ecosystems) (Colas et
62 al., 2019; Filbee-Dexter et al., 2022; Tiegs et al., 2024; Vyšná et al., 2014). Like other standardized
63 substrates used in decomposition studies (e.g., litter bags), cotton-strips quantify organic-matter-
64 decomposition potential, that is, the capacity of the ecosystem to decompose organic matter, rather
65 than the actual rate of native organic-matter decomposition *in situ*. A standard approach is to place
66 them in the field for a known amount of time, retrieve them, and measure the loss in tensile strength, as
67 a measure of the degree of decomposition. This approach has revealed many factors that impact
68 decomposition in streams such as temperature, land use, aqueous chemistry, sediment texture, stream
69 flow, location within the stream network, and canopy cover, among others (Griffiths and Tiegs, 2016;
70 Tiegs et al., 2024).

71 Studies have examined the relationship between organic-matter decomposition and whole-stream
72 respiration (Mancuso et al., 2023; Pingram et al., 2020; Young and Collier, 2009), but have not
73 specifically tied organic-matter decomposition within sediments to sediment-associated respiration. This
74 leads to an open question and the focus of our study: To what degree are point-scale rates of organic-
75 matter-decomposition potential within sediments linked to reach-scale respiration associated with the
76 whole-stream ecosystem (ER_{tot}), the sediments (ER_{sed}), or the water column (ER_{wc})? ER_{tot} represents
77 reach-scale aerobic respiration from autotrophs and heterotrophs across benthic, planktonic, and
78 hyporheic zones. ER_{sed} comprises reach-scale sediment-associated respiration from benthic and
79 streambed sediments, rooted and submerged plants, and hyporheic zones that are hydrologically

80 connected to the active channel; ER_{wc} constitutes reach-scale planktonic respiration occurring only in
81 the water column.

82 We specifically tested the hypothesis that reach-scale ER_{sed} rates are strongly linked to point-scale
83 measurements of organic-matter decomposition within streambed sediments. More specifically, we
84 tested the prediction that cotton-strip-decay rates are best explained by ER_{sed} , with little additional
85 variation in decay rates explained by ER_{tot} or ER_{wc} . To test our hypothesis and associated prediction we
86 used field deployments across the Yakima River Basin (YRB). The YRB is an environmentally diverse basin
87 in southeastern Washington State (USA) that is $\sim 16,000$ km² and with a stream network that culminates
88 in the 7th-order Yakima River. To generate the data needed to test our hypothesis, we used a
89 combination of sensors and cotton strips across 48 sites in the YRB that collectively spanned a
90 continuum from small mountainous streams in coniferous forests with little human impact to a large
91 lowland river in an arid environment surrounded by significant agricultural land use. The resulting
92 patterns help to fill a fundamental knowledge gap in our understanding of how point-scale organic-
93 matter-decomposition potential relates to reach-scale respiration and can be used to inform models
94 that aim to mechanistically integrate biogeochemical processes within and across stream networks.

95

96 **Methods**

97 To evaluate the linkages between organic-matter decomposition and stream ecosystem respiration we
98 took advantage of a prior study (Garayburu-Caruso et al., 2025) that separated ER_{tot} , ER_{sed} , and ER_{wc}
99 across environmentally divergent locations in the YRB (Fig. 1). Garayburu-Caruso et al. (2025) used
100 dissolved oxygen (DO) sensors, dark bottle incubations, and the single-station method (Odum, 1956) to
101 estimate these three components of respiration. In addition, that study deployed sensors to log water
102 temperature, used here to calculate cumulative degree days as described below. These and associated
103 contextual data were downloaded from existing data packages (Delgado et al., 2023; Forbes et al., 2023;
104 Garayburu-Caruso et al., 2023), and methods are described in detail by Garayburu-Caruso et al. (2025).
105 In brief, DO timeseries were analyzed via StreamMetabolizer (Appling et al., 2018) to estimate ER_{tot} . The
106 length of the reach that a given DO sensor integrates varies across streams and has been
107 estimated to be roughly three times the turnover length of O₂ (Hall and Hotchkiss, 2017b). As such,
108 integrated reach lengths likely varied across sites due to differences in reaeration and discharge.
109 Field sites were located in separate, non-overlapping reaches, helping to minimize potential spatial
110 autocorrelation between neighboring sites in the estimated metabolic rates. To estimate ER_{wc} , 2 L
111 opaque bottles containing a DO sensor were filled with stream water and incubated *in situ*; the rate of
112 DO drawdown was used as the estimate of ER_{wc} . The difference between ER_{tot} and ER_{wc} was used as an
113 estimate of ER_{sed} , which represents all respiration in the stream system that is not directly occurring in
114 the water column. ER_{sed} therefore includes respiration in the hyporheic zone, the streambed surface,
115 and rooted/submerged plants. We note, however, that ER estimates derived from open diel O₂ methods
116 capture all oxygen-consuming processes, not solely aerobic respiration. These estimates could also
117 include abiotic oxidation of dissolved Fe(II) or the oxidation of other end products from anaerobic
118 metabolism (Demars et al., 2015; Piatka et al., 2021), other oxidation processes such as nitrification and
119 photooxidation of organic matter (Demars et al., 2015; Estapa and Mayer, 2010), or O₂ inputs from
120 groundwater (Hall and Tank, 2005). Because ER_{sed} was calculated by the difference between ER_{tot} and
121 ER_{wc} , it may be sensitive to these non-respiratory O₂ sinks. However, biological metabolism is generally
122 considered the dominant O₂-consuming pathway in streams and we therefore interpret ER_{sed} primarily

123 as sediment-associated biological O₂ consumption while acknowledging that other contributions may be
124 captured.

125 To take advantage of the ecosystem respiration study, cotton strips made of Artist fabric (following the
126 protocol of Tiegs et al., 2013) were deployed at the same time as the DO sensors. They were deployed
127 upstream of the DO sensors to capture the upstream reach that influenced the DO sensor readings and
128 prevent disturbance during sensor maintenance. This design prioritized among-reach coverage across
129 the basin (48 sites) and provided point-scale estimates of decomposition potential at a single location
130 within each reach.

131 The cotton strips were deployed in the shallow hyporheic zone for 35 continuous days at 48 sites across
132 the YRB (Fig. 1). At each site, deployment locations were selected to be representative of the reach in
133 terms of sediment size, flow velocity, and substrate composition. In larger river systems (e.g., 7th-order
134 reaches), deployments were limited to wadeable areas near channel margins. Deployment and retrieval
135 days varied across four days, but all strips were deployed for 35 days: deployments were from July 25th
136 to July 28th, 2022 and retrievals were from August 29th to September 1st, 2022. Cotton strips were cut
137 from bolts of 12-ounce, heavy-weight cotton fabric composed of 95% cellulose (Style 548; Fredrix,
138 Lawrenceville, GA, USA). Each strip was 27 threads wide and cut to 8.0 cm by 2.5 cm (after Tiegs et al.
139 2013). Each cotton strip was laid flat in a stainless-steel mesh cage (10.8 x 4.5 cm, RSV Jumbo Mesh Herb
140 Infuser) to minimize physical damage and feeding by macroinvertebrates, thereby emphasizing microbe-
141 based decomposition. At each site, four cages with one strip each were attached to the underside of
142 clay bricks (20 x 10 x 5.5 cm) with stainless steel wire. The brick/cage/strip setup was nestled into
143 streambed sediment such that the cages/strips were within the sediments and the brick was at the
144 sediment/water interface. The four cages were next to each other. This setup kept the cotton strips out
145 of direct light and within the sediments while allowing water to flow past the cotton strips.

146 After the 35-day incubation period, cotton strips were carefully removed from cages and gently brushed
147 with gloved hands in stream water for approximately 10 s to remove large debris. Cleaned cotton strips
148 were placed in 50 mL conical centrifuge tubes with 70% ethanol. Tubes were capped and rolled
149 approximately 10 times before ethanol was removed. After completing this step, clean 70% ethanol was
150 added to the 50 mL tube to minimize further microbial-based decomposition. Cotton strips were
151 transported in the ethanol filled tubes on blue ice to Pacific Northwest National Laboratory in Richland,
152 WA. At the laboratory, the ethanol was removed from the tubes and cotton strips were air dried
153 overnight prior to further drying in an oven at 40 °C for at least 24 hours. After drying, cotton strips were
154 stored in air-tight containers with desiccant.

155 Dried cotton strips were shipped to Oakland University, Rochester, MI for tensile-strength analysis
156 following the protocol in Tiegs et al., (2013). A tensiometer was used to estimate tensile strength (Mark
157 10 MG100 with a Chatillon TCM 201 with roller jaws). The tensiometer pulled each cotton strip at a rate
158 of 2 cm/min. Some of the cotton strips were completely degraded such that there was no material to
159 measure, while other cages only contained fragments that were too small to measure tensile strength.
160 These non-detect strips accounted for 5.4% of all deployed strips. In both cases, a limit of detection was
161 assigned as the lowest tensile strength calculated in Tiegs et al. (2019) divided by 2, resulting in a final
162 value of 0.05. This was done to avoid statistical artifacts that can arise when simply introducing a value
163 of 0 (i.e., the natural log transformation in Equation 1 would be undefined). Removing these strips
164 entirely would bias the analyses away from conditions with very fast decomposition.

165 Tensiometer data were converted into decay rates using tensile loss calculated via Equation 1 (as in
166 Mancuso et al., 2022).

$$167 \quad K = \frac{-\ln(T_s/T_{sc})}{Time} \quad \text{Equation 1}$$

168 Here, K is the decomposition rate, T_s is the post-incubation tensile strength of the deployed cotton
169 strips, and T_{sc} is the mean tensile strength of control strips that were not incubated in the field. The time
170 variable was calculated as either the number of chronological deployment days (i.e., 35 days) or the
171 number of degree days. Using degree days as the time variable accounts for variation in temperature
172 across field sites and was estimated separately for each site as the sum of mean daily river temperature
173 over the incubation period. We use K_{cd} and K_{dd} to represent decay rate per chronological day or per
174 degree day, respectively. The values of K_{cd} and K_{dd} were estimated for each individual cotton strip and
175 then replicates were averaged to provide a single site-level value for K_{cd} and K_{dd} .

176 We examined both K_{cd} and K_{dd} to evaluate whether the connection between decomposition and reach-
177 scale respiration rates depends on accounting for temperature variation across the study basin. This is
178 particularly relevant in the YRB because our field sites ranged from colder headwater streams to warmer
179 low-gradient rivers. To test our hypothesis, we conducted both univariate and multivariate regression-
180 based analyses. We used ordinary least squares regression to examine the strength of univariate
181 correlations between K_{cd} or K_{dd} and ER_{tot} , ER_{wc} , or ER_{sed} . We complemented this univariate analysis with
182 multiple regression analysis to find an optimized model to explain variation in either K_{cd} or K_{dd} .

183 Further, to explore how other system variables may explain variation in decomposition rates, a LASSO
184 (Least Absolute Shrinkage and Selection Operator) regression model was built using physical, chemical
185 and environmental variables (Table S1) as inputs, and K_{cd} or K_{dd} as the response variables. Variables were
186 cube root transformed and z-score normalized to reduce the impact of high leverage points in the
187 regression analysis and to equally weight all variables. The LASSO regression was performed over 100
188 iterations, each with a different random seed using the `cv.glmnet` function in the `glmnet` R package
189 (Friedman et al., 2010). β coefficients were normalized to the maximum β coefficient for each iteration,
190 then averaged over the 100 iterations for the final reported value. Both the raw and normalized mean β
191 coefficient and standard deviation are reported in addition to the R^2 (Table 2).

192

193 **Results and Discussion**

194 **Decomposition in the Yakima River Basin spans globally reported rates**

195 Both K_{cd} and K_{dd} exhibited a wide range of values (Fig. 2), effectively spanning the theoretical maximum
196 of what could have been observed with our deployment setup. This is evidenced by some cotton strips
197 being completely consumed prior to retrieval (5.4% of all strips, K_{cd} and K_{dd} maximized), while others
198 were largely intact (K_{cd} and $K_{dd} \approx 0$). This variation is surprising given the relatively small spatial domain
199 sampled by this study, and emphasizes that environmental heterogeneity can surpass the effects of
200 spatial extent (Mancuso et al., 2022). The environments studied here ranged from pristine locations in
201 the mountainous headwaters of the YRB to lowland locations with heavy agricultural influences (Fig. 1;
202 Laan et al. 2025). This emphasizes the value of environmentally diverse watersheds like the YRB as
203 useful testbeds to study variation in decomposition rates within single hydrologically connected basins.

204 Comparing decay rates from the YRB to a global dataset from > 500 streams and rivers (Tiegs et al.,
205 2024) showed that YRB rates spanned nearly the entire global range and had substantial overlap with
206 the bulk of the global distributions (Fig. 2a,b). Dominant peaks in the YRB rate distributions were shifted
207 slightly towards faster rates, relative to primary peaks in the global dataset (Fig. 2a,b). This shift towards
208 faster rates and the wide range in rates are likely due to several factors linked to rates being estimated
209 in later summer with high temperatures, and established biological communities due to several months
210 since high-flow disturbances (Collier et al., 2013b; Grimm and Fisher, 1989; Mancuso et al., 2023). The
211 two decay rates were also closely correlated with each other, though the relationship weakened
212 towards locations with faster decay rates (**Fig. 2c**). This suggests a weak influence of temperature in the
213 YRB; a strong influence of temperature should lead to a weak relationship between K_{cd} and K_{dd} . These
214 results contrast previously reported influences of temperature on particulate organic-matter
215 decomposition (Benbi et al., 2014; Griffiths and Tiegs, 2016), and likely reflect dominance of other
216 influential factors such as variation in nutrient concentrations (Rosemond et al. 2015). Temperature-
217 driven decomposition is also expected to lead to a strong relationship between K_{cd} and summed
218 temperature, but we observed a very weak relationship despite ~4-fold variation in summed
219 temperature (**Fig. 2d**). This range in temperature among sites would likely be smaller in other seasons,
220 and we do not therefore expect a strong influence of temperature to emerge in the YRB by conducting
221 the study in other seasons. These results emphasize the need to understand factors governing variation
222 in decay rates across the YRB. This is especially true given that rate distributions within this one basin
223 span nearly all globally observed decay rates.

224 Across the YRB there appears to be potential for some spatial organization for both K_{cd} and K_{dd} (**Fig. 3**).
225 Visual inspection of the maps suggests that the spatial organization may be stronger for K_{cd} than for K_{dd} .
226 To evaluate this possibility more rigorously, we regressed each decay rate against upstream drainage
227 area (Fig. 4). In this case, drainage area is meant to reflect position within the YRB. We used drainage
228 area in preference to stream order because it is a continuous variable directly tied to the spatial domain
229 a given stream integrates, whereas stream order is categorical and primarily reflects stream network
230 topology. Associated regressions were significant ($p < 0.05$) with both decay rates increasing with
231 drainage area (**Fig. 4**). The relationship with drainage area was stronger, in terms of R^2 , for K_{cd} . Both
232 relationships were, however, relatively weak with R^2 values of 0.22 and 0.14 for K_{cd} and K_{dd} , respectively
233 (**Fig. 4**). Nonetheless, the existence of a significant relationship after controlling for temperature (i.e., for
234 K_{dd}) indicates that spatially structured factors other than temperature influence decay rates. This is not
235 surprising as studies using cotton strips have found several factors that influence decomposition, such as
236 nutrient concentrations, turbidity, and many others (Collier et al., 2013b; Pingram et al., 2020; Tiegs et
237 al., 2024). Before exploring a broad suite of potential explanatory variables, we tested our hypothesis
238 that decomposition rates will be better explained by sediment-associated respiration (ER_{sed}) than by
239 respiration in the water column (ER_{wc}) or by respiration of the integrated stream system (ER_{tot}).

240

241 **Respiration in sediments explains little variation in decomposition**

242 Contrary to our hypothesis, we found that both decay rates were most strongly connected to ER_{tot} , less
243 so with ER_{sed} , and not at all with ER_{wc} (**Fig. 5**). Univariate models using ER_{tot} were better than multivariate
244 models using ER_{sed} , ER_{wc} , and their interaction. This is evidenced by univariate models using ER_{tot} having
245 AIC values more than two units lower than multivariate models containing ER_{sed} and ER_{wc} (**Table 1**).

246 Multivariate models were not used with ER_{tot} because it contains ER_{sed} and ER_{wc} . Garayburu-Caruso et
247 el., 2025 showed that ER_{sed} accounted for the majority of ER_{tot} across most of the YRB, with 88% of
248 locations showing ER_{sed} contributions exceeding 50% of ER_{tot} . The strong correspondence between these
249 two metrics might explain the similar R^2 values observed. We note, however, that the difference in
250 explained variance between ER_{tot} ($R^2 = 0.29$ for K_{cd} ; $R^2 = 0.16$ for K_{dd}) and ER_{sed} ($R^2 = 0.22$ for K_{cd} ; $R^2 = 0.13$
251 for K_{dd}) was modest, and the stronger association with ER_{tot} should be interpreted cautiously.

252 To interpret these results, we note that cotton strips were deployed a few centimeters into the riverbed
253 sediments, beneath a brick set flush with the streambed surface. We conceptualized this deployment as
254 the shallow hyporheic zone, which was a reason we hypothesized that decay rates would be most
255 strongly connected to ER_{sed} . However, the results indicate that point-scale decomposition of particulate
256 organic matter within the shallow hyporheic zone is linked to respiratory processes occurring in both the
257 sediment and water column. Therefore, our deployment depth might have reflected sediment-water
258 interface processes in addition to shallow hyporheic zone processes, leading to stronger associations of
259 cotton strip decomposition with ER_{tot} . We also note that ER_{sed} estimates may not exclusively reflect
260 biological respiration, as non-respiratory O_2 -consuming processes can contribute to these estimates (see
261 Methods). We propose that if our deployment configuration was complemented with a simultaneous
262 deployment that enabled growth of benthic algal biofilms on the cotton strips, the combined
263 decomposition from both deployments could, in some systems, capture more of the processes that
264 contribute to ER_{sed} . This would provide a more complete view of sediment-associated biogeochemical
265 function, potentially leading to a stronger correlation between decomposition rates and ER_{sed} . While this
266 remains to be tested, the underlying idea is that primary producers support a large portion of
267 respiration associated with riverbed sediments, which is supported by recent analyses showing a strong
268 link between ER_{sed} and gross primary production across the YRB (Garayburu-Caruso et al., 2025).

269 **Slower rates of K_{cd} and K_{dd} are in streams with coarse sediments, set within wet forests**

270 Given that our hypothesis was rejected and that ER_{tot} explained only about 29% and 16% of K_{cd} and K_{dd} ,
271 respectively (**Table 1, Figure 5**), we used a discovery-based approach to explore other system variables
272 that may explain further variation in decomposition rates. LASSO-based modeling indicated that total
273 dissolved nitrogen (TDN) and the median grain size of sediment texture (D50) were most important for
274 explaining K_{dd} , while TDN and aridity were most important for explaining K_{cd} (**Table 2**). Other variables
275 were retained in the LASSO models (**Table S1**), but we interpreted TDN, D50, and aridity as the most
276 important because they consistently had the largest normalized coefficients. This interpretation is based
277 on these variables having mean normalized coefficients above 0.5—in terms of absolute value—
278 meaning they were at least 50% as important as the most important variable in the 100 LASSO model
279 runs. Further, the LASSO coefficients for these variables had a coefficient of variation less than 0.5,
280 meaning that across the 100 LASSO model runs the values of their normalized coefficients were
281 relatively stable (**Table S1**). The LASSO modeling also confirmed a relatively weak influence of
282 temperature, evidenced by relatively small and highly variable β coefficients for summed temperature in
283 the K_{cd} model (Table S1); temperature was not used in the K_{dd} model.

284 Both decomposition rates increased with higher TDN concentrations, while K_{dd} decreased with larger
285 D50 and K_{cd} decreased with higher aridity index values (**Table 1**). To more deeply interpret these
286 relationships, we examined Pearson-based univariate correlations between these three explanatory
287 variables and other variables included in the LASSO models. This is important because of strong

288 collinearity among some explanatory variables (**Fig. S1**). In this case, variables identified as being the
289 most important may be acting as proxies for one or more additional variables. We found that TDN was
290 most strongly correlated with percent agricultural land cover of the upstream drainage area and sulfate
291 concentrations in the stream water (**Fig. S1**). Increases in both decomposition rates with TDN may,
292 therefore, reflect agricultural inputs of nutrients that increase overall microbial activity of the stream
293 ecosystems we studied. D50 was most strongly correlated with the aridity index, which was most
294 strongly correlated with percent forest cover; the correlation between D50 and aridity is unlikely to
295 reflect a causal connection, while aridity and forest cover most likely are causally linked. If the
296 relationship between decomposition and D50 is causal, it could be mediated by the total surface area
297 available for microbial attachment. This would, however, influence decomposition only to the extent
298 that microbial biomass in adjacent sediments impacts microbial activity on the cotton strips. Coarser
299 sediments have much less surface area, potentially limiting overall microbial activity.

300 Considering the directionality of the univariate relationships, in context of the LASSO outcomes,
301 suggests slower decomposition—for both rates—in streams with relatively coarse sediments and set
302 within relatively wet forests. This contrasts with Clapcott and Barmuta (2010) who found faster
303 decomposition in coarser sediments. The discrepancy is likely because we excluded macroinvertebrates
304 while they did not, and they interpreted the link to sediment texture as due to greater habitat
305 availability for macroinvertebrates in coarser sediments. Locations with slower decomposition should,
306 thus, primarily be in higher elevation, relatively pristine parts of the YRB, while faster decomposition
307 occurs at lower elevations impacted by agricultural inputs. These results are consistent with previous
308 work showing greater cotton strip decomposition in impaired streams (Young and Collier, 2009), those
309 with little natural land cover (Collier et al., 2013a; Webb et al., 2019), and in streams with higher
310 nutrient concentrations (Ferreira et al., 2015; Pingram et al., 2020; Tiegs et al., 2013). In addition to
311 differences in nutrient concentrations between higher and lower elevation sites, we expect less light
312 penetration to streams in higher elevation sites because of more forest cover and smaller streams.
313 Though not measured here, less light could suppress autotrophic production which may limit
314 heterotrophic respiration (Bernhardt et al., 2022; Mulholland et al., 2001; Young and Huryn, 1999).
315 Lower autotrophic production could therefore slow decomposition relative to high-light conditions by
316 reducing the supply of labile carbon from phototrophs that can prime organic-matter degradation
317 (Danger et al. 2013; Howard-Parker et al. 2020).

318 **Point-scale decomposition is associated with processes across the sediment-water continuum and** 319 **land features**

320 Our results collectively indicate that to study shallow hyporheic zone decomposition processes, it is not
321 sufficient to conceptualize organic-matter decomposition by only considering sediment or water column
322 processes; one must examine the integrated system. The implication of our analyses is that point-scale
323 organic-matter decomposition potential was more closely associated with integrated system respiration
324 than with individual respiration components. Our findings suggest that mechanistic models of stream
325 ecosystem respiration may benefit from accounting for sediment processes, water-column processes,
326 and land-cover influences from beyond the stream. Focusing exclusively on the hyporheic zone is
327 insufficient, even in systems for which the hyporheic zone accounts for most reactions (Boano et al.,
328 2014; Burrows et al., 2017; McClain et al., 2003). This is further emphasized by previous work showing
329 that most respiration occurs in the water column of large rivers (Gardner and Doyle, 2018; Roley et al.,
330 2023). Garayburu-Caruso et al. (2025) also show that fractional contributions of ER_{sed} to ER_{tot} is often

331 high, but that there is significant variation in those fractional influences across the YRB. This variability is
332 due to ER_{wc} being fast enough, in some locations, to account for more than 80% of ER_{tot} (Garayburu-
333 Caruso et al., 2025). Similarly, Laan et al. (2025) found substantial overlap between the distribution of
334 ER_{wc} rates from the YRB and ER_{tot} from across the contiguous United States. The overall picture is that
335 decomposition is the result of integrated processes occurring across the sediment-water continuum and
336 influenced by external factors tied to land cover and land use. We infer that these integrated processes
337 are influenced by biophysical variation across the YRB (Laan et al., 2025), leading to decomposition rates
338 within this single basin that resemble global rate distributions and nearly span the global range of
339 observed rates (Tiegs et al., 2024). Other basins that contain only one ecoregion or have homogeneous
340 land cover may be expected to have a narrower range of decomposition rates (Webb et al., 2019). We
341 note that our decomposition estimates represent point-scale conditions at wadeable locations and
342 should be interpreted as such rather than as reach-integrated measures of decomposition. Capturing
343 within-reach spatial variability in decomposition across habitats and channel depths would complement
344 the among-reach approach used here, and may lead to stronger relationships between decomposition
345 rates and reach-scale ER. Nonetheless, models applied to any stream network that aim to predict
346 spatiotemporal variation in decomposition rates would be well served by considering processes
347 throughout the integrated watershed system.

348 **Code and data availability**

349 Data and scripts used to generate the main findings within this manuscript can be found at
350 <https://github.com/river-corridors-sfa/rcsfa-ST-2B-SSS-cotton-strip>. Upon acceptance of this
351 manuscript, they will be published on the U.S. Department of Energy's Environmental System Science
352 Data Infrastructure for a Virtual Ecosystem (ESS-DIVE) repository. Other data collected during the field
353 efforts (i.e., sensor data; surface water chemistry data; and geospatial information, metadata, and maps
354 for 2021 Spatial Study sampling event) can be accessed on ESS-DIVE at [https://data.ess-](https://data.ess-dive.lbl.gov/datasets/doi:10.15485/1987520)
355 [dive.lbl.gov/datasets/doi:10.15485/1987520](https://data.ess-dive.lbl.gov/datasets/doi:10.15485/1987520) (Garayburu-Caruso et al., 2023), [https://data.ess-](https://data.ess-dive.lbl.gov/datasets/doi:10.15485/1969566)
356 [dive.lbl.gov/datasets/doi:10.15485/1969566](https://data.ess-dive.lbl.gov/datasets/doi:10.15485/1969566) (Delgado et al., 2023), and [https://data.ess-](https://data.ess-dive.lbl.gov/datasets/doi:10.15485/1923689)
357 [dive.lbl.gov/datasets/doi:10.15485/1923689](https://data.ess-dive.lbl.gov/datasets/doi:10.15485/1923689) (Forbes et al., 2023).

358 **Author contributions**

359 Conceptualization: JCS, MB, VAGC, PR, ST

360 Data Curation: MB, JCS, BF, ML, SM, DD, LR and AEG

361 Formal Analysis: MB, MML, BF, and JCS

362 Funding Acquisition: JCS

363 Investigation: MB, DD, BF, VAGC, AEG, ML, SM, PR, LR, ST and JCS

364 Methodology: MB, DD, BF, VAGC, AEG, ML, SM, PR, LR, ST and JCS

365 Project Administration: MB, VAGC and JCS

366 Resources: MB, DD, BF, VAGC, AEG, ML, SM, PR, LR, ST and JCS

367 Software: MB, MML, BF, and JCS

368 Supervision: MB, VAGC and JCS
369 Validation: MB and JCS
370 Visualization: MB, MML, BF, and JCS
371 Writing – Original Draft Preparation: MB, VAGC, ST and JCS
372 Writing – Review & Editing: MB, DD, BF, VAGC, AEG, ML, SM. PR, LR, ST and JCS
373 **Competing interest**
374 The authors declare that they have no conflict of interest.

375 **Acknowledgements**

376 This work was supported by the River Corridor Science Focus Area (RC-SFA) at the Pacific Northwest
377 National Laboratory (PNNL). The RC-SFA is supported by the United States Department of Energy, Office
378 of Biological and Environmental Research (BER), Environmental System Science (ESS) Program. PNNL is
379 operated by Battelle Memorial Institute for the United States Department of Energy under contract no.
380 DE-AC05-76RL01830. We thank the United States Forest Service, Washington Department of Natural
381 Resources, Washington Department of Fish and Wildlife, Confederated Tribes and Bands of the Yakama
382 Nation, and Cowiche Canyon Conservancy for access to field locations where these samples were
383 collected. We also thank the Confederated Tribes and Bands of the Yakama Nation Tribal Council and
384 Yakama Nation Fisheries for working with us to facilitate sample collection and optimization of data
385 usage according to their values and worldview. We thank the field team including: Dillman Delgado,
386 Morgan Barnes, Brandon T. Boehnke, Yunxiang Chen, Kali Cornwell, Brianna I. Gonzalez, Samantha
387 Grieger, Glenn E. Hammond, Peishi Jiang, Bing Li, Zhi Li, Xinming Lin, Sophia A. McKeever, Maruti K.
388 Mudunuru, Katherine A. Muller, Opal Otenburg, Aaron Pelly, Kelsey Peta, Alan Roebuck, Joshua M.
389 Torgeson, and Jianqiu Zheng.
390

391 **References**

392 Allan, J. D., Castillo, M. M., and Capps, K. A.: Stream Ecology: Structure and Function of Running Waters,
393 Springer International Publishing, Cham, <https://doi.org/10.1007/978-3-030-61286-3>, 2021.

394 Appling, A. P., Hall Jr., R. O., Yackulic, C. B., and Arroita, M.: Overcoming Equifinality: Leveraging Long
395 Time Series for Stream Metabolism Estimation, *Journal of Geophysical Research: Biogeosciences*, 123,
396 624–645, <https://doi.org/10.1002/2017JG004140>, 2018.

397 Battin, T. J., Lauerwald, R., Bernhardt, E. S., Bertuzzo, E., Gener, L. G., Hall, R. O., Hotchkiss, E. R.,
398 Maavara, T., Pavelsky, T. M., Ran, L., Raymond, P., Rosentreter, J. A., and Regnier, P.: River ecosystem
399 metabolism and carbon biogeochemistry in a changing world, *Nature*, 613, 449–459,
400 <https://doi.org/10.1038/s41586-022-05500-8>, 2023.

401 Benbi, D. K., Boparai, A. K., and Brar, K.: Decomposition of particulate organic matter is more sensitive to
402 temperature than the mineral associated organic matter, *Soil Biology and Biochemistry*, 70, 183–192,
403 <https://doi.org/10.1016/j.soilbio.2013.12.032>, 2014.

404 Benfield, E. F., Fritz, K. M., and Tiegs, S. D.: Chapter 27 - Leaf-Litter Breakdown, in: *Methods in Stream Ecology (Third Edition)*, edited by: Lamberti, G. A. and Hauer, F. R., Academic Press, 71–82,
405 <https://doi.org/10.1016/B978-0-12-813047-6.00005-X>, 2017.

407 Bernhardt, E. S., Savoy, P., Vlah, M. J., Appling, A. P., Koenig, L. E., Hall, R. O., Arroita, M., Blaszcak, J. R.,
408 Carter, A. M., Cohen, M., Harvey, J. W., Heffernan, J. B., Helton, A. M., Hosen, J. D., Kirk, L., McDowell,
409 W. H., Stanley, E. H., Yackulic, C. B., and Grimm, N. B.: Light and flow regimes regulate the metabolism of
410 rivers, *Proceedings of the National Academy of Sciences*, 119, e2121976119,
411 <https://doi.org/10.1073/pnas.2121976119>, 2022.

412 Boano, F., Harvey, J. W., Marion, A., Packman, A. I., Revelli, R., Ridolfi, L., and Wörman, A.: Hyporheic
413 flow and transport processes: Mechanisms, models, and biogeochemical implications, *Reviews of*
414 *Geophysics*, 52, 603–679, <https://doi.org/10.1002/2012RG000417>, 2014.

415 Boulton, A. J., Findlay, S., Marmonier, P., Stanley, E. H., and Valett, H. M.: The functional significance of
416 the hyporheic zone in streams and rivers, *Annual Review of Ecology, Evolution, and Systematics*, 29, 59–
417 81, <https://doi.org/10.1146/annurev.ecolsys.29.1.59>, 1998.

418 Burrows, R. M., Rutledge, H., Bond, N. R., Eberhard, S. M., Auhl, A., Andersen, M. S., Valdez, D. G., and
419 Kennard, M. J.: High rates of organic carbon processing in the hyporheic zone of intermittent streams,
420 *Sci Rep*, 7, 13198, <https://doi.org/10.1038/s41598-017-12957-5>, 2017.

421 Clapcott, J. E. and Barmuta, L. A.: Metabolic patch dynamics in small headwater streams: exploring
422 spatial and temporal variability in benthic processes, *Freshwater Biology*, 55, 806–824,
423 <https://doi.org/10.1111/j.1365-2427.2009.02324.x>, 2010.

424 Colas, F., Woodward, G., Burdon, F. J., Guérol, F., Chauvet, E., Cornut, J., Cébron, A., Clivot, H., Danger,
425 M., Danner, M. C., Pagnout, C., and Tiegs, S. D.: Towards a simple global-standard bioassay for a key
426 ecosystem process: organic-matter decomposition using cotton strips, *Ecological Indicators*, 106,
427 105466, <https://doi.org/10.1016/j.ecolind.2019.105466>, 2019.

428 Cole, J. J., Prairie, Y. T., Caraco, N. F., McDowell, W. H., Tranvik, L. J., Striegl, R. G., Duarte, C. M.,
429 Kortelainen, P., Downing, J. A., Middelburg, J. J., and Melack, J.: Plumbing the Global Carbon Cycle:
430 Integrating Inland Waters into the Terrestrial Carbon Budget, *Ecosystems*, 10, 172–185,
431 <https://doi.org/10.1007/s10021-006-9013-8>, 2007.

432 Collier, K. J., Clapcott, J. E., Hamer, M. P., and Young, R. G.: Extent estimates and land cover relationships
433 for functional indicators in non-wadeable rivers, *Ecological Indicators*, 34, 53–59,
434 <https://doi.org/10.1016/j.ecolind.2013.04.010>, 2013a.

435 Collier, K. J., Clapcott, J. E., Duggan, I. C., Hamilton, D. P., Hamer, M., and Young, R. G.: Spatial Variation
436 of Structural and Functional Indicators in a Large New Zealand River, *River Research and Applications*,
437 29, 1277–1290, <https://doi.org/10.1002/rra.2609>, 2013b.

438 Delgado, D., Barnes, M., Boehnke, B. T., Chen, X., Chen, Y., Cornwell, K., Forbes, B., Fulton, S. G.,
439 Garayburu-Caruso, V. A., Goldman, A. E., Gonzalez, B. I., Grieger, S., Hammond, G. E., Jiang, P., Kaufman,
440 M. H., Laan, M., Li, B., Li, Z., Lin, X., McKeever, S. A., Mudunuru, M. K., Muller, K. A., Myers-Pigg, A.,
441 Otenburg, O., Pelly, A., Peta, K., Powers-McCormack, B., Regier, P., Renteria, L., Roebuck, A., Scheibe, T.
442 D., Son, K., Torgeson, J. M., Zheng, J., and Stegen, J. C.: Spatial Study 2022: Surface Water Samples,

443 Cotton Strip Degradation, and Hydrologic Sensor Data across the Yakima River Basin, Washington, USA
444 (v3), 2023.

445 Demars, B. O. L., Thompson, J., and Manson, J. R.: Stream metabolism and the open diel oxygen method:
446 Principles, practice, and perspectives, *Limnology and Oceanography: Methods*, 13, 356–374,
447 <https://doi.org/10.1002/lom3.10030>, 2015.

448 Drake, T. W., Raymond, P. A., and Spencer, R. G. M.: Terrestrial carbon inputs to inland waters: A current
449 synthesis of estimates and uncertainty, *Limnology and Oceanography Letters*, 3, 132–142,
450 <https://doi.org/10.1002/lo2.10055>, 2018.

451 Estapa, M. L. and Mayer, L. M.: Photooxidation of particulate organic matter, carbon/oxygen
452 stoichiometry, and related photoreactions, *Marine Chemistry*, 122, 138–147,
453 <https://doi.org/10.1016/j.marchem.2010.06.003>, 2010.

454 Fellows, C. S., Valett, M. H., and Dahm, C. N.: Whole stream metabolism in two montane streams:
455 Contribution of the hyporheic zone, *Limnology and Oceanography*, 46, 523–531,
456 <https://doi.org/10.4319/lo.2001.46.3.0523>, 2001.

457 Ferreira, V., Castagneyrol, B., Koricheva, J., Gulis, V., Chauvet, E., and Graça, M. A. S.: A meta-analysis of
458 the effects of nutrient enrichment on litter decomposition in streams, *Biological Reviews*, 90, 669–688,
459 <https://doi.org/10.1111/brv.12125>, 2015.

460 Filbee-Dexter, K., Feehan, C. J., Smale, D. A., Krumhansl, K. A., Augustine, S., Bettignies, F. de, Burrows,
461 M. T., Byrnes, J. E. K., Campbell, J., Davoult, D., Dunton, K. H., Franco, J. N., Garrido, I., Grace, S. P.,
462 Hancke, K., Johnson, L. E., Konar, B., Moore, P. J., Norderhaug, K. M., O’Dell, A., Pedersen, M. F.,
463 Salomon, A. K., Sousa-Pinto, I., Tiegs, S., Yiu, D., and Wernberg, T.: Kelp carbon sink potential decreases
464 with warming due to accelerating decomposition, *PLOS Biology*, 20, e3001702,
465 <https://doi.org/10.1371/journal.pbio.3001702>, 2022.

466 Forbes, B., Barnes, M., Boehnke, B. T., Bowden, M. E., Chen, X., Cornwell, K., Crawford, M., Delgado, D.,
467 Fulton, S. G., Garayburu-Caruso, V. A., Gary, S., Goldman, A. E., Gonzalez, B. I., Grieger, S., Hammond, G.
468 E., Jiang, P., Kaufman, M. H., Laan, M., Li, B., Li, Z., McKeever, S. A., Mudunuru, M. K., Muller, K. A., Myers-
469 Pigg, A., Ocejo, J. A., Otenburg, O., Pelly, A., Peta, K., Powers-McCormack, B., Regier, P., Renteria, L.,
470 Roebuck, A., Scheibe, T. D., Son, K., Tffaily, M. M., Torgeson, J. M., Stegen, J. C., and Consortium, T. W.:
471 WHONDRS River Corridor Sediment and Water Geochemistry and In Situ Sensor Data from Machine-
472 Learning-Informed Sites across the Contiguous United States (v6), 2023.

473 Friedman, J., Hastie, T., and Tibshirani, R.: Regularization Paths for Generalized Linear Models via
474 Coordinate Descent, *Journal of Statistical Software*, 33, 1–22, <https://doi.org/10.18637/jss.v033.i01>,
475 2010.

476 Garayburu-Caruso, V. A., Kaufman, M. H., Delgado, D., Barnes, M., Boehnke, B. T., Chen, X., Cornwell, K.,
477 Forbes, B., Fulton, S. G., Goldman, A. E., Gonzalez, B. I., Grieger, S., Jr, R. O. H., Hammond, G. E., Jiang, P.,
478 Laan, M., Li, B., Li, Z., Lin, X., McKeever, S. A., Mudunuru, M. K., Muller, K. A., Myers-Pigg, A., Otenburg,
479 O., Pelly, A., Peta, K., Regier, P., Renteria, L., Roebuck, A., Scheibe, T. D., Son, K., Torgeson, J. M., and
480 Stegen, J. C.: Spatial Study 2022: Water Column, Sediment, and Total Ecosystem Respiration Rates across
481 the Yakima River Basin, Washington, USA (v2), 2023.

482 Garayburu-Caruso, V. A., Kaufman, M., Forbes, B., Hall, R. O., Laan, M., Chen, X., Lin, X., Fulton, S.,
483 Renteria, L., Fang, Y., Son, K., and Stegen, J. C.: Sediment-associated processes account for most of the
484 spatial variation in ecosystem respiration in the Yakima River basin, *bioRxiv*, 2024.03.22.586339,
485 <https://doi.org/10.1101/2024.03.22.586339>, 2025.

486 Gardner, J. R. and Doyle, M. W.: Sediment–Water Surface Area Along Rivers: Water Column Versus
487 Benthic, *Ecosystems*, 21, 1505–1520, <https://doi.org/10.1007/s10021-018-0236-2>, 2018.

488 Griffiths, N. A. and Tiegs, S. D.: Organic-matter decomposition along a temperature gradient in a
489 forested headwater stream, *Freshwater Science*, 35, 518–533, 2016.

490 Grimm, N. B. and Fisher, S. G.: Stability of Periphyton and Macroinvertebrates to Disturbance by Flash
491 Floods in a Desert Stream, *Journal of the North American Benthological Society*, 8, 293–307,
492 <https://doi.org/10.2307/1467493>, 1989.

493 Hall, R. O. and Hotchkiss, E. R.: Chapter 34 - Stream Metabolism, in: *Methods in Stream Ecology* (Third
494 Edition), edited by: Lamberti, G. A. and Hauer, F. R., Academic Press, 219–233,
495 <https://doi.org/10.1016/B978-0-12-813047-6.00012-7>, 2017a.

496 Hall, R. O. and Hotchkiss, E. R.: Stream Metabolism, in: *Methods in Stream Ecology*, Academic Press,
497 219–233, <https://doi.org/10.1016/B978-0-12-813047-6.00012-7>, 2017b.

498 Hall, R. O. and Tank, J. L.: Correcting whole-stream estimates of metabolism for groundwater input,
499 *Limnology and Oceanography: Methods*, 3, 222–229, <https://doi.org/10.4319/lom.2005.3.222>, 2005.

500 Krause, S., Hannah, D. M., Fleckenstein, J. H., Heppell, C. M., Kaeser, D., Pickup, R., Pinay, G., Robertson,
501 A. L., and Wood, P. J.: Inter-disciplinary perspectives on processes in the hyporheic zone, *Ecohydrology*,
502 4, 481–499, <https://doi.org/10.1002/eco.176>, 2011.

503 Laan, M. M., Fulton, S. G., Garayburu-Caruso, V. A., Barnes, M. E., Borton, M. A., Chen, X., Farris, Y.,
504 Forbes, B., Goldman, A. E., Grieger, S., Hall Jr., R. O., Kaufman, M. H., Lin, X., Zionce, E. L. M., McKeever, S.
505 A., Myers-Pigg, A., Otenburg, O., Pelly, A. C., Ren, H., Renteria, L., Scheibe, T. D., Son, K., Tagestad, J.,
506 Torgeson, J. M., and Stegen, J. C.: Water column respiration in the Yakima River basin is explained by
507 temperature, nutrients, and suspended solids, *Biogeosciences*, 22, 6137–6152,
508 <https://doi.org/10.5194/bg-22-6137-2025>, 2025.

509 Lewandowski, J., Arnon, S., Banks, E., Batelaan, O., Betterle, A., Broecker, T., Coll, C., Drummond, J. D.,
510 Gaona Garcia, J., Galloway, J., Gomez-Velez, J., Grabowski, R. C., Herzog, S. P., Hinkelmann, R., Höhne,
511 A., Hollender, J., Horn, M. A., Jaeger, A., Krause, S., Löchner Prats, A., Magliozzi, C., Meinikmann, K.,
512 Mojarrad, B. B., Mueller, B. M., Peralta-Maraver, I., Popp, A. L., Posselt, M., Putschew, A., Radke, M.,
513 Raza, M., Riml, J., Robertson, A., Rutere, C., Schaper, J. L., Schirmer, M., Schulz, H., Shanafield, M., Singh,
514 T., Ward, A. S., Wolke, P., Wörman, A., and Wu, L.: Is the Hyporheic Zone Relevant beyond the Scientific
515 Community?, *Water*, 11, 2230, <https://doi.org/10.3390/w11112230>, 2019.

516 Mancuso, J., Messick, E., and Tiegs, S. D.: Parsing spatial and temporal variation in stream ecosystem
517 functioning, *Ecosphere*, 13, e4202, <https://doi.org/10.1002/ecs2.4202>, 2022.

518 Mancuso, J., Tank, J. L., Mahl, U. H., Vincent, A., and Tiegs, S. D.: Monthly variation in organic-matter
519 decomposition in agricultural stream and riparian ecosystems, *Aquat Sci*, 85, 83,
520 <https://doi.org/10.1007/s00027-023-00975-7>, 2023.

521 McClain, M. E., Boyer, E. W., Dent, C. L., Gergel, S. E., Grimm, N. B., Groffman, P. M., Hart, S. C., Harvey,
522 J. W., Johnston, C. A., Mayorga, E., McDowell, W. H., and Pinay, G.: Biogeochemical Hot Spots and Hot
523 Moments at the Interface of Terrestrial and Aquatic Ecosystems, *Ecosystems*, 6, 301–312, 2003.

524 Mulholland, P. J., Fellows, C. S., Tank, J. L., Grimm, N. B., Webster, J. R., Hamilton, S. K., Martí, E.,
525 Ashkenas, L., Bowden, W. B., Dodds, W. K., McDowell, W. H., Paul, M. J., and Peterson, B. J.: Inter-biome
526 comparison of factors controlling stream metabolism, *Freshwater Biology*, 46, 1503–1517,
527 <https://doi.org/10.1046/j.1365-2427.2001.00773.x>, 2001.

528 Naegeli, M. W. and Uehlinger, U.: Contribution of the hyporheic zone to ecosystem metabolism in a
529 prealpine gravel-bed-river, *Journal of the North American Benthological Society*, 16, 794–804, 1997.

530 Odum, H. T.: Primary production in flowing waters 1, *Limnology and oceanography*, 1, 102–117, 1956.

531 Piatka, D. R., Wild, R., Hartmann, J., Kaule, R., Kaule, L., Gilfedder, B., Peiffer, S., Geist, J., Beierkuhnlein,
532 C., and Barth, J. A. C.: Transfer and transformations of oxygen in rivers as catchment reflectors of
533 continental landscapes: A review, *Earth-Science Reviews*, 220, 103729,
534 <https://doi.org/10.1016/j.earscirev.2021.103729>, 2021.

535 Pingram, M. A., Clapcott, J. E., Hamer, M. P., Atalah, J., and Özkundakci, D.: Exploring temporal and
536 spatial variation in cotton tensile-strength loss to assess the ecosystem health of non-wadeable rivers,
537 *Ecological Indicators*, 108, 105773, <https://doi.org/10.1016/j.ecolind.2019.105773>, 2020.

538 Roley, S. S., Hall Jr., R. O., Perkins, W., Garayburu-Caruso, V. A., and Stegen, J. C.: Coupled primary
539 production and respiration in a large river contrasts with smaller rivers and streams, *Limnology and*
540 *Oceanography*, 68, 2461–2475, <https://doi.org/10.1002/lno.12435>, 2023.

541 Talluto, L., del Campo, R., Estévez, E., Altermatt, F., Datry, T., and Singer, G.: Towards (better) fluvial
542 meta-ecosystem ecology: a research perspective, *npj biodiversity*, 3, 1–10,
543 <https://doi.org/10.1038/s44185-023-00036-0>, 2024.

544 Tank, J. L., Rosi-Marshall, E. J., Griffiths, N. A., Entekin, S. A., and Stephen, M. L.: A review of
545 allochthonous organic matter dynamics and metabolism in streams, *Journal of the North American*
546 *Benthological Society*, 29, 118–146, 2010.

547 Tiegs, S. D., Clapcott, J. E., Griffiths, N. A., and Boulton, A. J.: A standardized cotton-strip assay for
548 measuring organic-matter decomposition in streams, *Ecological Indicators*, 32, 131–139,
549 <https://doi.org/10.1016/j.ecolind.2013.03.013>, 2013.

550 Tiegs, S. D., Costello, D. M., Isken, M. W., Woodward, G., McIntyre, P. B., Gessner, M. O., Chauvet, E.,
551 Griffiths, N. A., Flecker, A. S., Acuña, V., Albariño, R., Allen, D. C., Alonso, C., Andino, P., Arango, C.,
552 Aroviita, J., Barbosa, M. V. M., Barmuta, L. A., Baxter, C. V., Bell, T. D. C., Bellinger, B., Boyero, L., Brown,
553 L. E., Bruder, A., Bruesewitz, D. A., Burdon, F. J., Callisto, M., Canhoto, C., Capps, K. A., Castillo, M. M.,
554 Clapcott, J., Colas, F., Colón-Gaud, C., Cornut, J., Crespo-Pérez, V., Cross, W. F., Culp, J. M., Danger, M.,
555 Dangles, O., Eyto, E. de, Derry, A. M., Villanueva, V. D., Douglas, M. M., Elosegi, A., Encalada, A. C.,

556 Entrekin, S., Espinosa, R., Ethaiya, D., Ferreira, V., Ferriol, C., Flanagan, K. M., Fleituch, T., Shah, J. J. F.,
557 Frainer, A., Friberg, N., Frost, P. C., Garcia, E. A., Lago, L. G., Soto, P. E. G., Ghate, S., Giling, D. P., Gilmer,
558 A., Gonçalves, J. F., Gonzales, R. K., Graça, M. A. S., Grace, M., Grossart, H.-P., Guérol, F., Gulis, V.,
559 Hepp, L. U., Higgins, S., Hishi, T., Huddart, J., Hudson, J., Imberger, S., Iñiguez-Armijos, C., Iwata, T.,
560 Janetski, D. J., Jennings, E., Kirkwood, A. E., Koning, A. A., Kosten, S., Kuehn, K. A., Laudon, H., Leavitt, P.
561 R., Silva, A. L. L. da, Leroux, S. J., LeRoy, C. J., Lisi, P. J., MacKenzie, R., Marcarelli, A. M., Masese, F. O.,
562 McKie, B. G., Medeiros, A. O., Meissner, K., Miliša, M., Mishra, S., Miyake, Y., Moerke, A., et al.: Global
563 patterns and drivers of ecosystem functioning in rivers and riparian zones, *Science Advances*, 5,
564 eaav0486, <https://doi.org/10.1126/sciadv.aav0486>, 2019.

565 Tiegs, S. D., Capps, K. A., Costello, D. M., Schmidt, J. P., Patrick, C. J., Follstad Shah, J. J., Leroy, C. J., and
566 CELLDEX Consortium#: Human activities shape global patterns of decomposition rates in rivers, *Science*,
567 384, 1191–1195, 2024.

568 Vyšná, V., Dyer, F., Maher, W., and Norris, R.: Cotton-strip decomposition rate as a river condition
569 indicator – Diel temperature range and deployment season and length also matter, *Ecological Indicators*,
570 45, 508–521, <https://doi.org/10.1016/j.ecolind.2014.05.011>, 2014.

571 Webb, J. R., Pearce, N. J. T., Painter, K. J., and Yates, A. G.: Hierarchical variation in cellulose
572 decomposition in least-disturbed reference streams: a multi-season study using the cotton strip assay,
573 *Landscape Ecol*, 34, 2353–2369, <https://doi.org/10.1007/s10980-019-00893-w>, 2019.

574 Wondzell, S. M.: The role of the hyporheic zone across stream networks, *Hydrological Processes*, 25,
575 3525–3532, <https://doi.org/10.1002/hyp.8119>, 2011.

576 Woodward, G., Gessner, M. O., Giller, P. S., Gulis, V., Hladyz, S., Lecerf, A., Malmqvist, B., McKie, B. G.,
577 Tiegs, S. D., and Cariss, H.: Continental-scale effects of nutrient pollution on stream ecosystem
578 functioning, *Science*, 336, 1438–1440, 2012.

579 Young, R. G. and Collier, K. J.: Contrasting responses to catchment modification among a range of
580 functional and structural indicators of river ecosystem health, *Freshwater Biology*, 54, 2155–2170,
581 <https://doi.org/10.1111/j.1365-2427.2009.02239.x>, 2009.

582 Young, R. G. and Huryn, A. D.: Effects of Land Use on Stream Metabolism and Organic Matter Turnover,
583 *Ecological Applications*, 9, 1359–1376, [https://doi.org/10.1890/1051-
584 0761\(1999\)009%255B1359:EOLUOS%25D2.0.CO;2](https://doi.org/10.1890/1051-0761(1999)009%255B1359:EOLUOS%25D2.0.CO;2), 1999.

585 Zarnetske, J. P., Haggerty, R., Wondzell, S. M., and Baker, M. A.: Dynamics of nitrate production and
586 removal as a function of residence time in the hyporheic zone, *Journal of Geophysical Research:*
587 *Biogeosciences*, 116, <https://doi.org/10.1029/2010JG001356>, 2011.

588

589

590

591

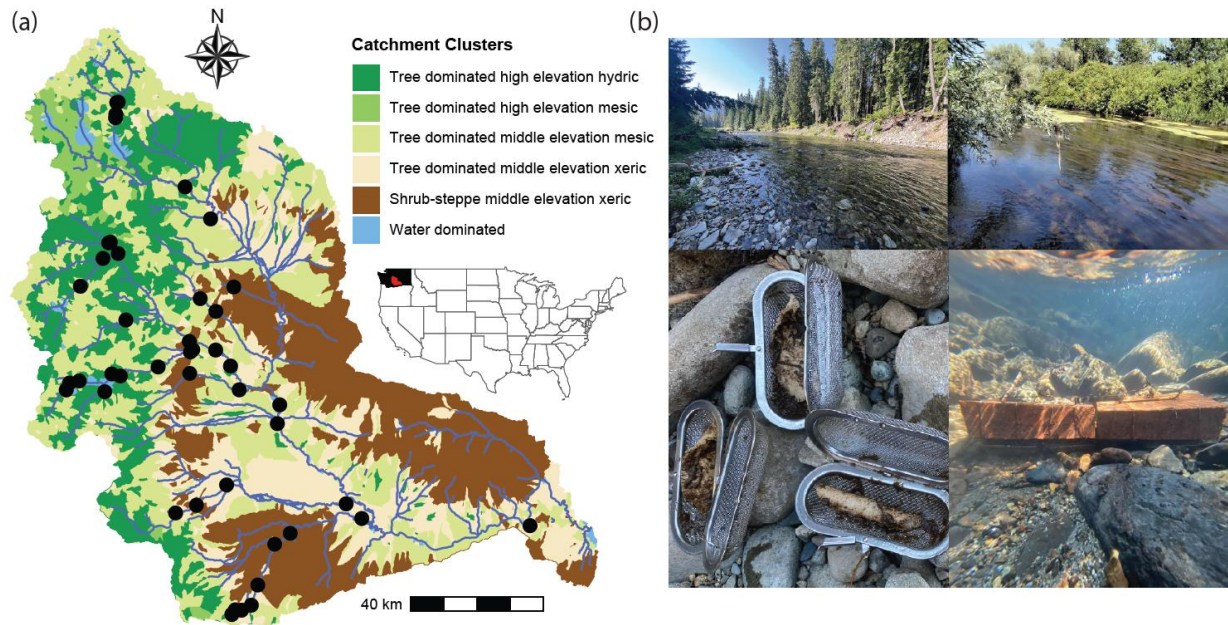
592

593

594

595

596 **Figures**

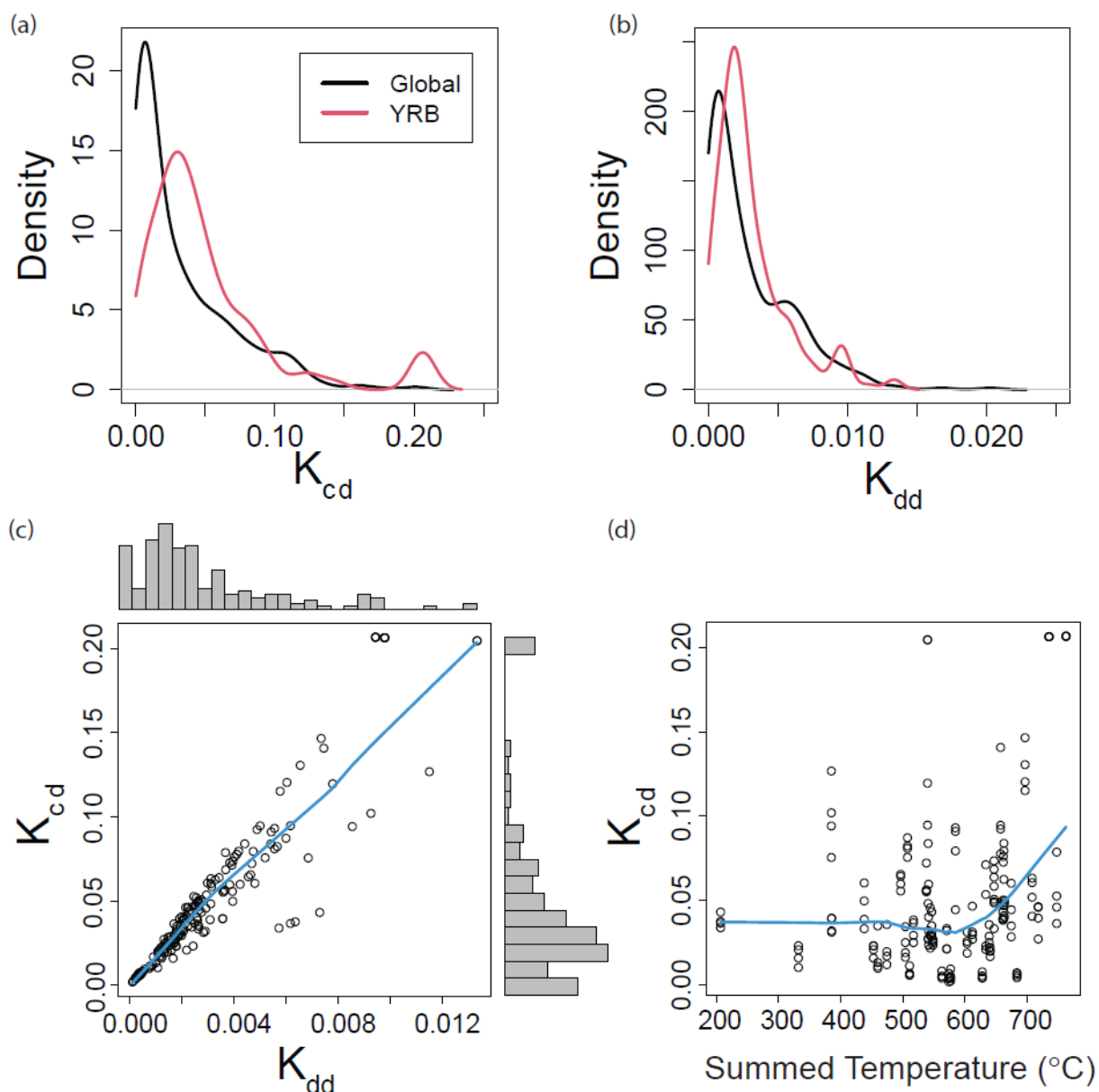


597

598 **Figure 1. Biophysical clusters, sampling locations, and example conditions across the YRB.** (a) The inset
599 map shows the location of the YRB within the contiguous United States, with black indicating
600 Washington State and red indicating the YRB. The YRB is shown with multiple colors, which correspond
601 to biophysical clusters, as presented in Laan et al. (2025) and summarized briefly in the legend. Black
602 circles are locations where decay rates were estimated. (b) Photos provide examples of the breadth of
603 conditions studied across the YRB, post-incubation states of cotton strips, and deployment of the cotton
604 strips.

605

606

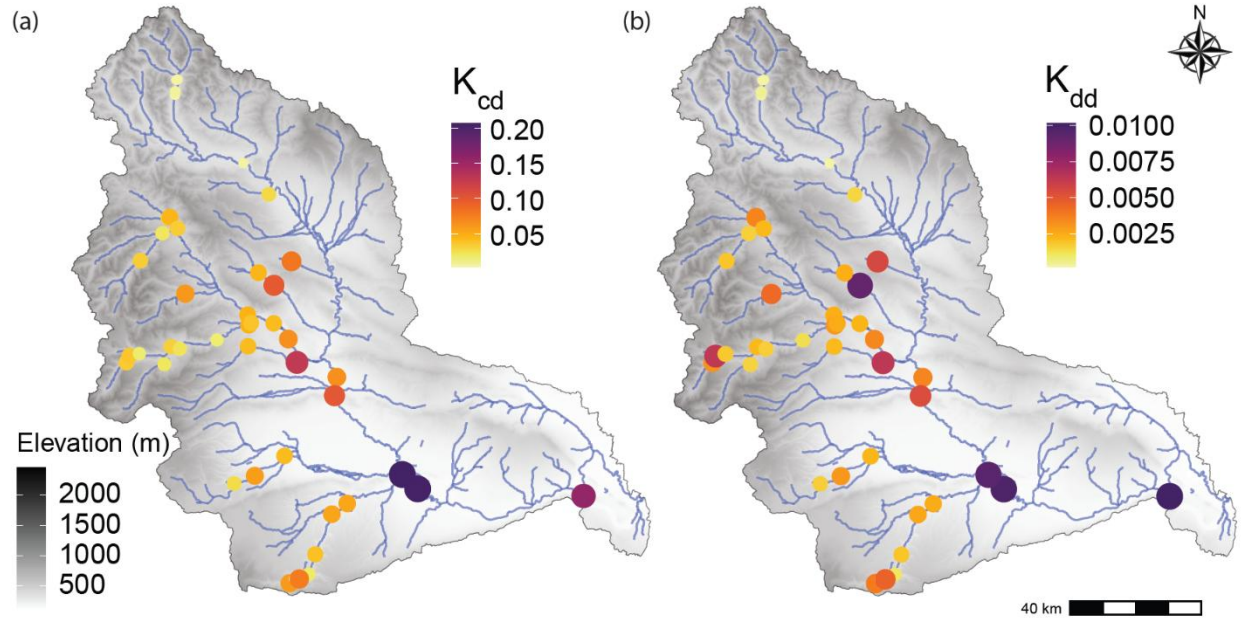


607

608 **Figure 2. Decay rate distributions and relationships to each other and temperature.** Kernel density
609 functions for (a) K_{cd} and (b) K_{dd} from a global streams and rivers dataset and from the YRB. (c) Scatterplot
610 correlating K_{cd} to K_{dd} . Histograms summarizing the distribution of each rate are provided on the outer
611 boundaries. (d) K_{cd} related to temperature summed across the deployment period; summed
612 temperature was used to calculate K_{dd} . Blue lines represent Lowess spline fits as regression analysis was
613 not required for interpretation.

614

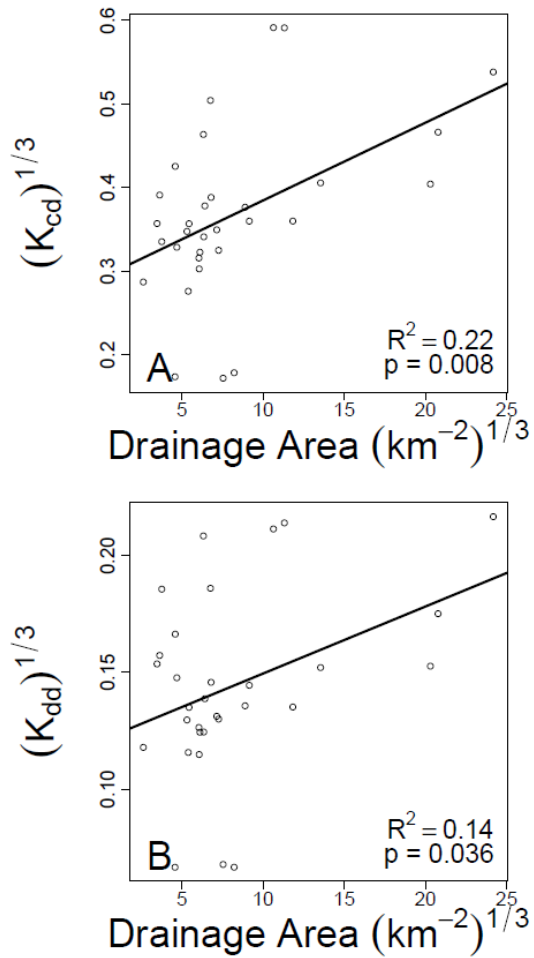
615



616

617 **Figure 3: Spatial distribution of decay rates across the YRB.** Each map shows elevation profiles and
 618 either K_{cd} (A) or K_{dd} (B). Colored circles are field locations where rates were estimated. The color of each
 619 circle is related to decay rate as indicated in the legends, and circle size is scaled to decay rate to further
 620 facilitate visual interpretability.

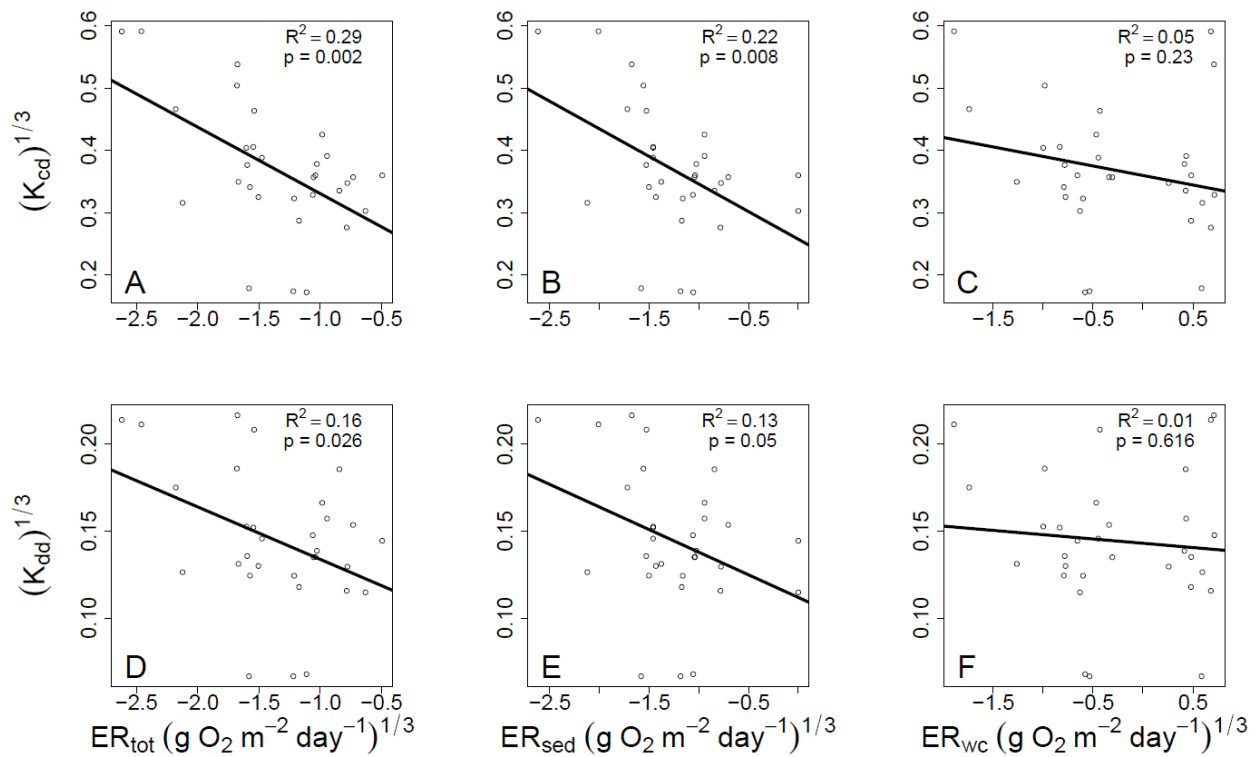
621



622

623 **Figure 4. Decay rates increase with drainage area.** K_{cd} (A) and K_{dd} (B) regressed against upstream
 624 drainage area and fit with an ordinary least squares linear regression. Associated regression models are
 625 shown as solid black lines and statistics are provided on each panel. Data were cube root transformed to
 626 improve normality before analysis.

627



629

630 **Figure 5: Decay rates related to each of the three aspects of stream ecosystem respiration.** Both K_{cd} (A-
 631 C) and K_{dd} (D-F) show strongest relationships with ER_{tot} (A,D), weaker relationships with ER_{sed} (B,E), and
 632 non-significant relationships with ER_{wc} (C,F). Ordinary least squares linear regression models are shown
 633 with solid black lines and associated statistics are provided on each panel. All variables were cube-root
 634 transformed to improve normality prior to regression analysis.

635

636 **Tables**

637 **Table 1.** Comparison of univariate and multivariate regression models explaining variation in K_{cd} and K_{dd} .
 638 Model structures are indicated, along with change in AIC relative to the best model. ER_{tot} was not used
 639 in multivariate models because $ER_{tot} = ER_{sed} + ER_{wc}$. Regression statistics for the univariate models are
 640 provided in Figure 5; only the best performing univariate models, in terms of R^2 , are shown. The models
 641 with ER_{sed} and ER_{wc} , but not the interaction term, are effectively the same as the ER_{tot} model because
 642 $ER_{tot} = ER_{sed} + ER_{wc}$. They are included as a point of reference for the model that also includes the
 643 $ER_{sed} * ER_{wc}$ interaction term.

Model	Δ AIC
$K_{cd} \sim ER_{tot}$	0
$K_{cd} \sim ER_{sed} + ER_{wc}$	3.8
$K_{cd} \sim ER_{sed} + ER_{wc} + ER_{sed} * ER_{wc}$	5.7
$K_{dd} \sim ER_{tot}$	0
$K_{dd} \sim ER_{sed} + ER_{wc}$	3.0
$K_{dd} \sim ER_{sed} + ER_{wc} + ER_{sed} * ER_{wc}$	4.8

644

645 **Table 2.** Regression coefficients from LASSO models explaining variation in K_{dd} and K_{cd} . Explanatory
 646 variables were cube root transformed to reduce influence from high leverage data points and
 647 standardized as z-scores to enable direct comparison of the regression coefficients. LASSO models were
 648 fit over 100 seeds. Regression coefficients (β) and R^2 values were averaged across the 100 seeds.
 649 Normalized regression coefficients were calculated by dividing each β coefficient by the maximum β
 650 coefficient in each seed. Standard deviation (sd) is reported for each variables' coefficient over the 100
 651 seeds and used to calculate the coefficient of variation (cv). Variables shown have an absolute value of
 652 mean normalized β of > 0.5 and $cv < 0.5$ to emphasize variables that were consistently important across
 653 seeds. Results for all variables, both normalized and not normalized, can be found in Table S1.

Response Variable	Predictor Variable	Mean Normalized Regression Coefficient (β)	sd	cv
K_{dd}	Water TDN	1	0	0
	D50	-0.699	0.087	-0.124
Mean R^2			0.502 (sd = 0.0673)	
K_{cd}	Aridity	-0.959	0.065	-0.067
	Water TDN	0.805	0.156	0.193
Mean R^2			0.883 (sd = 0.083)	

654

655

656

657

658